Research Article

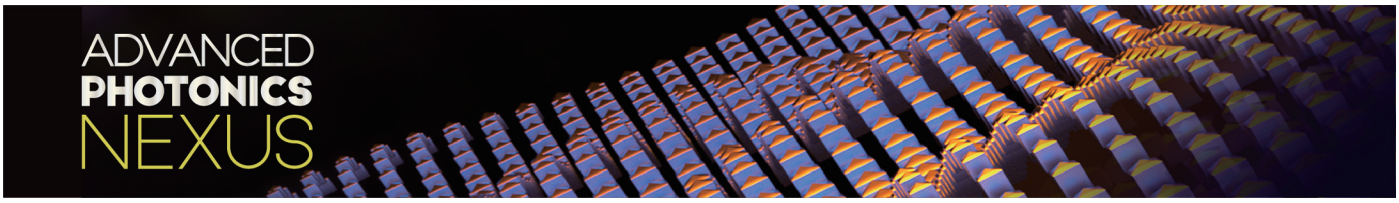

Generation of tunable high-order Laguerre–Gaussian petal-like modes from a mid-infrared optical vortex parametric oscillator

Yuxia Zhou,[a,b] Xining Yang,[b] Jianqiang Ye,[b] Yuanyuan Ma,[c,*] Ying Wan,[d] Jianxiang Wen,[e] and Taximaiti Yusufu[b,*]

[a]Xinjiang Normal University, School of Chemistry and Chemical Engineering, Urumqi, China
[b]Xinjiang Normal University, School of Physics and Electronic Engineering, Xinjiang Key Laboratory for Luminescence Minerals and Optical Functional Materials, Urumqi, China
[c]Chiba University, Graduate School of Engineering, Chiba, Japan
[d]Nanjing University of Information Science and Technology, School of Physics and Optoelectronic Engineering, Jiangsu Key Laboratory for Optoelectronic Detection of Atmosphere and Ocean, Nanjing, China
[e]Shanghai University, School of Communication and Information Engineering, Key Lab of Specialty Fiber Optics and Optical Access Networks, Shanghai, China

Abstract. High-order Laguerre–Gaussian (LG) petal-like beams have become a topic of significant interest due to their potential application in next-generation optical trapping, quantum optics, and materials processing technologies. In this work, we demonstrate the generation of high-order LG beams with petal-like spatial profiles and tunable orbital angular momentum (OAM) in the mid-infrared wavelength region. These beams are generated using idler-resonant optical parametric oscillation (OPO) in a $KTiOAsO_4$ (KTA) crystal. By adjusting the length of the resonant cavity, the OAM of the mid-infrared idler field can be tuned and we demonstrate tuning in the range of 0 to ± 10. When using a maximum pump energy of 20.2 mJ, the maximum output energy of high-order modes $LG_{0,\pm 5}$, $LG_{0,\pm 8}$, and $LG_{0,\pm 10}$ were 0.8, 0.53, and 0.46 mJ, respectively. The means by which high-order LG modes with petal-like spatial profiles and tunable OAM were generated from the OPO is theoretically modeled by examining the spatial overlap efficiency of the beam waists of the pump and resonant idler fields within the center of the KTA crystal. The methodology presented in this work offers a simple and flexible method to wavelength-convert laser emission and generate high-order LG modes.

Keywords: high-order Laguerre–Gaussian petal-like modes; optical parametric oscillator; nonlinear optics; $KTiOAsO_4$; optical vortices.

Received Jan. 24, 2024; revised manuscript received Mar. 20, 2024; accepted for publication Apr. 22, 2024; published online Jun. 12, 2024.

[DOI: 10.1117/1.APN.3.3.036013]

1 Introduction

Optical vortex laser beams possess a phase singularity and a helical wavefront that twists in the beam's direction of propagation. Every photon of a vortex beam carries orbital angular momentum (OAM) of ℓh, which can be expressed as a phase factor $\exp(i\ell\varphi)$ (where φ is an azimuthal angle).[1–3] The unique characteristics of these beams have enabled new techniques in fields including optical tweezing,[4,5] optical manipulation,[6,7] optical communication,[8] nano/microfabrication of helical structured materials,[9] and spectroscopy.[10,11] Laguerre–Gaussian (LG) modes are eigensolutions of the Helmholtz equation under cylindrical symmetry, which can be directly generated from a laser cavity. LG modes are examples of vortex beams. High-order LG modes that have spatial profiles with petal-like

*Address all correspondence to Taximaiti Yusufu, taxmamat_84@sina.com; Yuanyuan Ma, mayuanyuan612@gmail.com

features across their azimuth are an important subset of LG modes. These modes have garnered significant attention for their use in manipulation of microparticles,[12,13] spatial measurement,[14] and quantum communication.[15] Therefore, significant research effort has focused on developing methods whereby high-order LG modes with petal-like spatial profiles that can be selectively generated from a laser system.

One approach for generating these types of LG modes is the coherent superposition of two optical vortex modes with opposite azimuthal order.[16] These modes can be generated directly within a laser cavity by controlling the gain/loss of specific cavity modes using intracavity phase modulating elements[17–19] and mode-selection approaches.[20,21] High-order LG modes with petal-like spatial profiles can also be generated by pumping a laser cavity with a ring-shaped pump beam that is slightly offset from the axis of the laser cavity. This method selectively promotes mode overlap between LG modes and the ring-shaped pump beam.[22,23] Another approach is to make use of defect spots and patterns within the laser cavity to force the oscillation of high-order LG modes.[24] More recently, researchers have used spherical aberration from a spherical lens to generate ultrahigh-order LG beams with ℓ order beyond 300 from an end-pump Nd: YVO_4 laser at 1064 nm; this is the highest-order LG mode with a petal-like spatial profile demonstrated from an experimental laser system.[25,26]

Nonlinear optical processes, such as stimulated Raman scattering, can be used to induce the generation of high-order LG modes.[27,28] It should be noted that there have been rather few reports of high-order LG mode generation in the mid-infrared wavelength region. The capacity to generate such modes in this wavelength range would be significant and have potential utility in next-generation optical trapping, quantum optics, and materials processing applications.

Optical parametric oscillation (OPO) is a nonlinear process, which has proven effective for the generation of optical vortex beams in the near-infrared and mid-infrared wavelength ranges.[29–34] There have however, been few reports concerning the generation of high-order LG petal-like modes in the mid-infrared wavelength range using OPOs. Recently, our group has demonstrated the generation of an off-axis vortex beam with noninteger OAM states from an OPO with a half-spherical cavity, resulting from the coherent superposition of Gaussian and vortex modes inside the cavity.[35]

In this paper, we report the first demonstration (to the best of our knowledge) of the generation of OAM-tunable high-order LG petal-like modes in the mid-infrared region from an idler-resonant $KTiOAsO_4$ (KTA)-OPO pumped by a nanosecond optical vortex source ($\ell_p = 1-3$). This cavity enables the selective generation of high-order $LG_{0,\pm\ell}$ ($\ell = 0-10$) petal-like modes (with controllable OAM) in the mid-infrared region by adjusting the cavity length. Our experimental work is supported by theoretical modeling that analyzes the spatial overlap efficiency of the beam waists of the pump and resonant idler fields within the center of the KTA crystal.

2 Experimental Methods

The experimental setup of the mid-infrared OPO generating high-order LG modes with petal-like spatial profiles is shown in Fig. 1. A flash lamp pumped Q-switched Nd:YAG laser that had a Gaussian output beam, pulse width of 25 ns, pulse repetition frequency of 50 Hz, and emission wavelength of 1064 nm was used as the pump source. A half-wave plate,

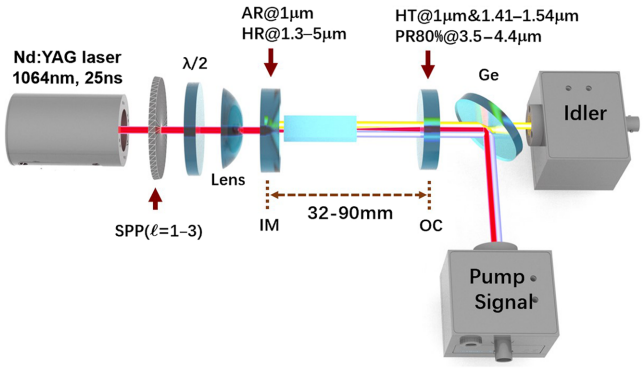

Fig. 1 Schematic showing the layout of the system used to generate mid-infrared high-order LG modes from a vortex-pumped optical parametric oscillator.

thin-film polarizer, and Faraday rotator (isolator) were used to control the power of the pump beam and prevent backreflection into the laser cavity. Multiple spiral phase plates (SPPs) (azimuthally divided into 16 parts with an $n\pi/8$ phase shift) were combined to convert the pump beam into an optical vortex beam. Using different arrangements of SPP, the topological charge ℓ of the pump beam could be changed from 1 to 3. A half-wave plate was used to adjust the polarization of the pump vortex beam so as to optimize phase matching within the OPO. Using a lens with a focal length $f = 750$ mm, the pump vortex beam was focused to a spot with a waist of 380 μm ($\ell_p = 1$), 474 μm ($\ell_p = 2$), and 510 μm ($\ell_p = 3$) at the center of the KTA crystal.

The idler-resonant KTA-OPO had a hemispherical cavity comprising a concave input mirror (IM) with a radius of curvature $R = 100$ mm and a plane output coupler (OC). The IM was antireflection-coated for 1.064 μm and high-reflection-coated for 1.3 to 5 μm ($R = 99\%$); the OC was coated partially reflecting ($R \approx 80\%$) for the idler beam and high-transmitting for the pump and signal beams. A type II noncritically phase-matched KTA crystal (x-cut, $\theta = 90$ deg, $\varphi = 0$ deg) with dimensions of 5 mm × 5 mm × 30 mm was used in the OPO. Both sides of the crystal were antireflection-coated for the pump, signal, and idler fields in order to minimize loss. The OC was mounted on a one-dimensional translation stage, and the geometrical length of the cavity (L) was varied in the range of 32 to 90 mm by moving the OC along the optical axis. The IM and KTA crystal were then fixed. A Ge filter was used to separate the idler output from the undepleted pump and signal outputs.

3 Results and Discussion

In these experiments, we first generated high-order $LG_{0,\pm\ell}$ modes with tunable topological charge by varying the resonant cavity length of the OPO. The spatial intensity profile of the pump beam was recorded using a CCD camera (Spiricon BGS-USB-SP620) and that of the signal and idler beams using a pyroelectric camera (Spiricon Pyrocam III, spatial resolution of 75 μm). When the OPO was pumped with a first-order optical vortex $\ell_p = 1$ [spatial profile shown in Fig. 2(a)], the signal field was generated with a similar spatial profile, as shown in Fig. 2(c). The OAM characteristics of the pump and signal beams were examined using the tilted lens method.[36] The spatial profiles of the pump and signal beams after being focused through the tilted lens are shown in Figs. 2(b) and 2(d),

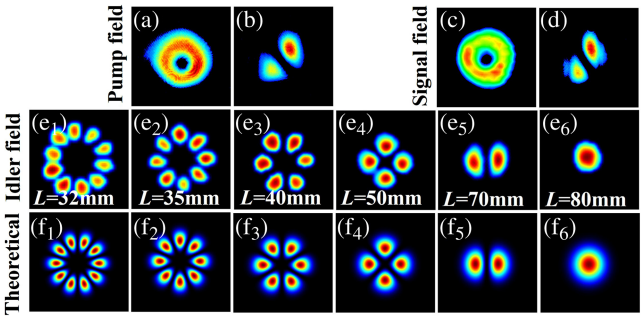

Fig. 2 Images showing the spatial intensity distribution of (a) the free-space and (b) focused (through a tilted lens) pump vortex beam with OAM = 1. Images of the spatial intensity distribution of (c) the free space and (d) focused (through a tilted lens) signal beam. (e_1)–(e_6) The experimentally obtained spatial profiles of the idler beam for a range of cavity lengths. (f_1)–(f_6) The corresponding theoretically modeled spatial intensity profiles of these beams.

respectively. In both cases, the presence of two lobes at the focal plane confirm the order of both the pump and the signal vortex beams to be $\ell = 1$. This result is in agreement with the conservation of OAM within an OPO wherein the OAM of the pump beam is transferred to the nonresonant signal beam. Generally, the idler beam should exhibit a Gaussian spatial profile, however, this was not always observed in this work. The spatial profile of the idler beam (as recorded using the pyroelectric camera) for a range of resonant cavity lengths is shown in Figs. 2(e1)–2(e6). It can be seen that the spatial intensity profile of the idler beam changes with the cavity length. Here, the order of the idler beam LG mode (and the number of petals in the spatial profile) can be increased by decreasing the length of the resonant cavity. The theoretically modeled spatial intensity profiles of the generated LG modes are shown for comparison in Figs. 2(f1)–2(f6). There have been a number of publications reporting the generation of similar mode shapes directly from a laser cavity.[37,38] These mode shapes can arise from the coherent superposition of LG modes with opposite azimuthal order oscillating within the laser cavity (such modes can freely oscillate within the cavity if no additional mode-control elements are used).

To further investigate the generation of high-order LG petal-like modes, the idler-resonant OPO was pumped using vortex beams with $\ell_p = 2$ and 3. When the OPO was pumped with a second-order vortex beam ($\ell = 2$) [free space and tilted lens focused spatial intensity profiles shown in Figs. 3(a) and 3(b), respectively], the generated signal beam was observed to have a doughnut-shaped intensity profile and carried an OAM of $\ell = 2$. The free-space and tilted lens-focused spatial intensity profiles of the generated signal beam are shown in Figs. 3(c) and 3(d), respectively. The results show that the signal field takes on the same OAM characteristics as the pump field; this characteristic was observed for all examined lengths of resonant cavity. The idler fields were generated in the form of high-order LG petal-like modes, and its OAM could be tuned from 0 to ± 8 by varying the length of the resonant cavity. The experimentally and theoretically and theoretically obtained spatial intensity profiles of the generated idler beams are shown in Fig. 3 for a range of resonant cavity lengths.

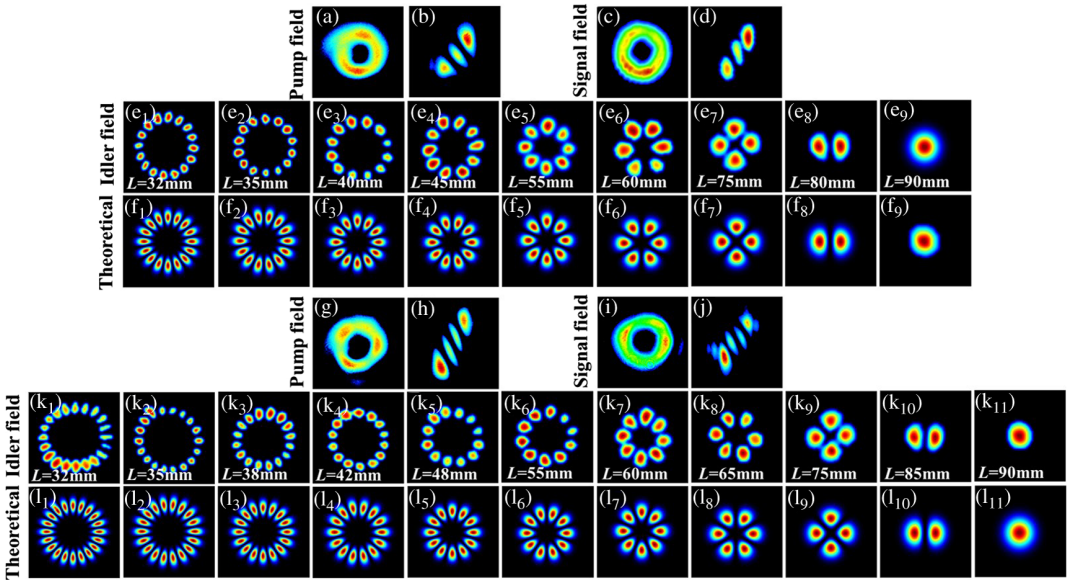

Fig. 3 A collection of images showing the spatial intensity profiles of modes generated when the OPO is pumped with vortex modes of order $\ell = 2$ and 3. (a) and (b) The free-space and focused (through a tilted lens) pump vortex beam with $\ell = 2$, respectively. (c) and (d) The corresponding profiles of the generated signal field. (e_1)–(e_9) The free-space spatial intensity profiles of the generated idler field, for a range of resonant cavity lengths. (f_1)–(f_9) The corresponding theoretically modeled mode profiles. (g) and (h) The free-pace and focused (through a tilted lens) pump vortex beam with $\ell = 3$, respectively. (i) and (j) The corresponding profiles of the generated signal field. (k_1)–(k_{11}) Free-space spatial intensity profiles of the generated idler field, for a range of resonant cavity lengths. (l_1)–(l_{11}) The corresponding theoretically modeled mode profiles.

When the OPO was pumped using an optical vortex of order ℓ_p of 3 [free-space and the tilted lens-focused spatial intensity profiles shown in Figs. 3(g) and 3(h), respectively], the generated signal beam was observed to have a doughnut-shaped intensity profile and carried an OAM of $\ell = 3$; this characteristic was observed for all investigated lengths of the resonant cavity. The free-space and tilted lens-focused spatial intensity profiles of the generated signal beam are shown in Figs. 3(i) and 3(j), respectively. By adjusting the length of the resonant cavity, the idler field could be generated in the form of high-order LG petal-like modes, and its OAM could be tuned from 0 to ±10. The experimentally obtained spatial intensity profiles of the generated idler fields are shown in Fig. 3 for a range of resonant cavity lengths.

The above results show that high-order LG modes with petal-like spatial profiles and tunable OAM can be generated directly from an idler-resonant KTA-OPO by adjusting the length of its resonant cavity. In fact, the handedness ($\pm\ell$) of LG mode with the same intensity profile cannot be well distinguished in the laser cavity, thereby resulting in the generation of petal-like modes formed of the coherent superposition of annular $LG_{0,+\ell}$ and $LG_{0,-\ell}$ modes. To better understand how these high-order LG modes were produced from this system, we performed theoretical modeling, wherein we examined the spatial overlap of the pump field with the cavity modes of the idler field within the resonant cavity of the OPO and the KTA crystal. The spatial overlap efficiency η of the pump intensity $I_p(r,z)$ and the cavity mode intensity $I_c(r,z)$ was modeled using the following equation:

$$\eta = \iint I_p(r,z) I_c(r,z) \mathrm{d}r\, \mathrm{d}z. \tag{1}$$

The normalized intensity distribution of an $LG_{0,\ell}$ mode can be expressed as[39]

$$I(r,\varphi,z) = \frac{2}{\pi w_0^2 dl!}\left[\frac{2r^2}{w_0^2}\right]^{|l|}\left[L_p^{|l|}\left(\frac{2r^2}{w_0^2}\right)\right]^2 \exp\left(\frac{-2r^2}{w_0^2}\right)\left\{\begin{matrix}\sin l\varphi \\ \cos l\varphi\end{matrix}\right\}^2, \tag{2}$$

where $L_p^{|\ell|}(\cdot)$ is the generalized Laguerre polynomial, and p and ℓ are the radial and azimuthal indices, respectively. d is the length of the gain medium, and w_0 is the cavity mode size, which is assumed to be constant in the laser crystal (along the axis of the laser).

If we consider a focused doughnut-shaped vortex pump beam, we can define the beam radius r_{outer} as the radius of a circle that contains 86.5% of the total energy of the beam, and the ring radius r_{inner} as the radius of the circle that contains 13.5% the total energy. The equation determining the spatial overlap efficiency can then be modified to[40]

$$\eta = \sum_{n=0}^{l}\frac{1}{(l-n)!}\left[\left(\frac{2r_{\mathrm{inner}}^2}{w_0^2}\right)^{l-n}\exp\left(-\frac{2r_{\mathrm{inner}}^2}{w_0^2}\right) - \left(\frac{2r_{\mathrm{outer}}^2}{w_0^2}\right)^{l-n}\exp\left(-\frac{2r_{\mathrm{outer}}^2}{w_0^2}\right)\right], \tag{3}$$

where the waist (w_0) of the fundamental cavity mode of a plano–concave linear cavity can be determined using[41]

$$w_0 = \sqrt{\frac{L_{\mathrm{eff}}\lambda}{\pi}}\left[\frac{g_1 g_2(1-g_1 g_2)}{(g_1+g_2-2g_1 g_2)^2}\right]^{1/4}, \tag{4}$$

where $L_{\mathrm{eff}} = L - (n_r - 1)d/n_r$ is the effective resonator length, λ is the wavelength of the lasing mode, n_r is the refractive index of the gain medium, $g_i = (1 - L_{\mathrm{eff}})/R_i$ is the g-factor of the resonator, and R is the radius of curvature of the cavity mirrors. The values of r_{inner} and r_{outer} were determined directly from our experiment. Here, the values of r_{inner} and r_{outer} for the pump vortex beams with $\ell_p = 1-3$ were 35.6 and 330 μm; 92.1 and 410 μm; and 132.8 and 440 μm, respectively. Using these values along with the above equations, we theoretically modeled the spatial overlap efficiency (η) as a function of the resonant cavity mode order (ℓ). These results are plotted in Fig. 4 for pump vortex beams with $\ell_p = 1-3$.

Figure 4 shows the calculated spatial overlap efficiency η between the vortex pump mode and high-order LG modes within the resonant cavity of the OPO at various cavity lengths (32 – 90 mm). When pumping with a vortex beam with order $\ell_p = 1$, the spatial overlap efficiency (red square) decreases monotonically as ℓ increases. When pumping with vortices of order, $\ell_p = 2$ and 3, the spatial overlap efficiency first increases and then decreases as the value of ℓ increases. The high-order LG mode, which is generated from the resonant cavity, is a function of both the intracavity loss of that mode and the spatial overlap of the pump field with that mode. Both of these factors are a function of the length of the resonant cavity. The output energies of the signal and idler beams were measured as a function of the pump energy when pumping with vortex beams of order $\ell_p = 1-3$ and for a range of resonant cavity lengths. These plots are shown in Fig. 5.

The plot of Fig. 5(a) shows that when using a pump field with $\ell_p = 1$ and an energy of 20.2 mJ, for cavity lengths of $L = 32$, 55, and 90 mm, the maximum output energies of the signal and idler fields were 2.9, 2.6, 2.1, and 0.8, 0.67, and 0.54 mJ, respectively. The corresponding slope efficiencies were 23.5%, 28.9%, 22.9%, and 6.4%, 7.4%, 6.2%, respectively. Figure 5(b) shows that the maximum output energies of the signal and idler fields when using a pump field with $\ell_p = 2$ for

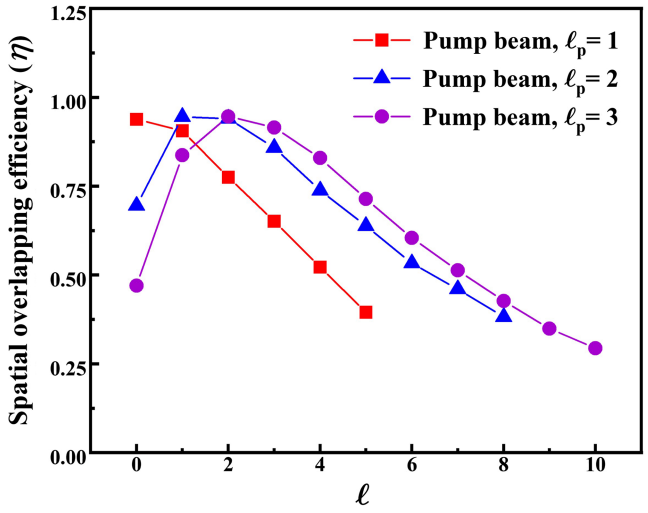

Fig. 4 Plots of the theoretically modeled spatial overlap efficiency as a function of resonant cavity mode order (ℓ) for pump vortex beams with topological charge ℓ_p of 1 – 3.

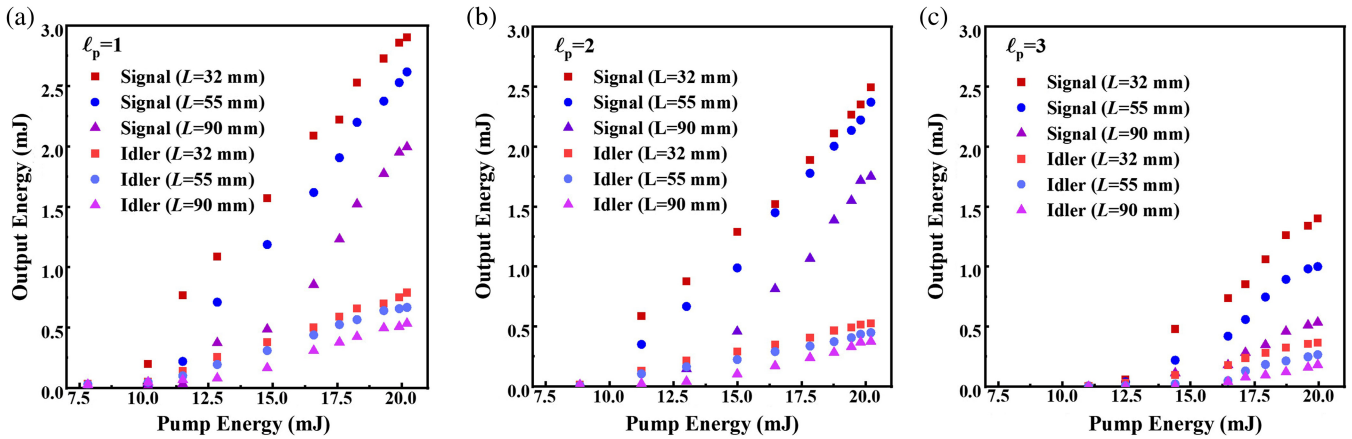

Fig. 5 Plots showing the output energies of the signal and high-order LG mode idler fields as a function of incident pump energy and for different resonant cavity lengths. Panel (a) shows results using a pump vortex beam with $\ell_p = 1$; panel (b) shows results using a pump vortex beam with $\ell_p = 2$; and panel (c) shows results using a pump vortex beam with $\ell_p = 3$.

cavity lengths of $L = 32$, 55, and 90 mm were 2.5, 2.3, 1.8, and 0.53, 0.45, 0.38 mJ, respectively. Figure 5(c) shows that the maximum output energies of the signal and idler fields when using a pump field with $\ell_p = 3$ for cavity lengths of $L = 32$, 55, and 90 mm were 1.4, 1, 0.54, and 0.37, 0.27, 0.18 mJ, respectively. The corresponding to slope efficiencies were 18.7%, 12.8%, 7.2%, 4.9%, 3.6%, and 2.4%, respectively. It should be noted that the oscillation threshold of high-order petal-like modes increases, as the extending of cavity length from 32 to 90 mm, which is due to the severe cavity loss. The measured oscillation threshold of OPO pumped by the optical vortex with order of, $\ell_p = 1 - 3$, were ranged within 7.7–10.2, 7.9–11.2, and 11.2–14.4 mJ, respectively. From these results, it is clear that pumping with the lowest order vortex mode yields the highest signal and idler output energies for a given pump energy and resonant cavity length.

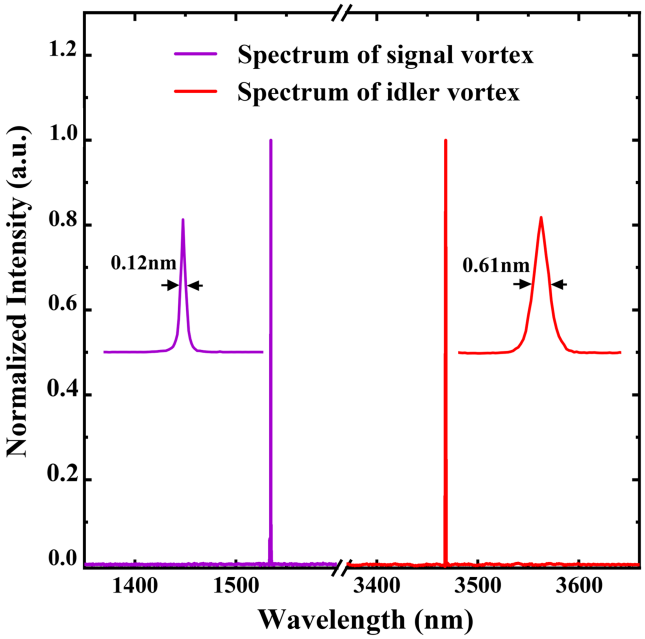

Fig. 6 Plots of the output signal (1535 nm) and idler (3468 nm) field spectra; insets are zoomed spectra highlighting the spectral bandwidth of each field.

The spectra of the signal and idler outputs (measured to be 1535 and 3468 nm, respectively) were recorded using a scanning monochromator (Spectra Pro HRS-500, 300 lines/mm, aperture size of 30 μm, spectral resolution of 0.3 to 0.4 nm in the wavelength range of 1000 to 5000 nm) and are plotted in Fig. 6. The spectral bandwidths of the signal and idler outputs were measured to be $\Delta\lambda_s \sim 0.32$ nm (ca. 1.36 cm^{-1}) and $\Delta\lambda_i \sim 0.67$ nm (ca. 0.56 cm^{-1})

4 Conclusions

We have demonstrated the generation of high-order $LG_{0,\pm\ell}$ mode idler field vortex beams with ℓ tunable from 0 to ± 10 using an idler-resonant KTA-OPO. The order of the output idler beam could be varied by adjusting the length of the resonant cavity and by changing the order of the vortex pump beam. A theoretical investigation of the spatial overlap efficiency of the pump vortex and resonant idler beams was undertaken to glean insight into the mechanism by which these high-order LG modes were generated. When pumped with vortex beams with $\ell = 1$, 2, and 3, due to the increase of spatial overlap efficiency, the highest-order idler beams that could be generated from the system were $LG_{0,\pm 5}$, $LG_{0,\pm 8}$, and $LG_{0,\pm 10}$, respectively. This work demonstrates the relative ease by which high-order LG laser modes in the mid-infrared wavelength range can be generated directly from an OPO system. We anticipate that such laser beams will have utility for applications in precise spatial measurements, optical trapping and tweezing, and free-space optical/quantum communications.

Disclosures

The authors declare no conflicts of interest.

Code and Data Availability

The data that support the findings of this study are available from the corresponding author upon reasonable request.

Acknowledgments

This work was supported by the National Natural Science Foundation of China (Grant Nos. 12264049 and 11664041) and the Xinjiang Normal University Young Outstanding Talent Programme (Grant No. XJNUQB2022-17).

References

1. L. Allen et al., "Orbital angular momentum of light and the transformation of Laguerre-Gaussian laser modes," *Phys. Rev. A* **45**(11), 8185–8189 (1992).
2. M. S. Soskin and M. V. Vasnetsov, "Singular optics," *Prog. Opt.* **42**(4), 219–276 (2001).
3. A. M. Yao and M. J. Padgett, "Orbital angular momentum: origins, behavior and applications," *Adv. Opt. Photonics* **3**(2), 161–204 (2011).
4. T. Omatsu et al., "Twisted materials: a new twist for materials science: the formation of chiral structures using the angular momentum of light," *Adv. Opt. Mater.* **7**(14), 1801672 (2019).
5. J. Chen, C. H. Wan, and Q. W. Zhan, "Engineering photonic angular momentum with structured light: a review," *Adv. Photonics* **3**(6), 064001 (2021).
6. D. G. Grier, "A revolution in optical manipulation," *Nature* **424**(6950), 810–816 (2003).
7. Y. J. Shen et al., "Optical vortices 30 years on: OAM manipulation from topological charge to multiple singularities," *Light Sci. Appl.* **8**(1), 1–29 (2019).
8. J. Wang, "Advances in communications using optical vortices," *Photonics Res.* **4**(5), B14–B28 (2016).
9. J. Ni et al., "Three-dimensional chiral microstructures fabricated by structured optical vortices in isotropic material," *Light Sci. Appl.* **6**(7), e17011 (2017).
10. M. Vainio and L. Halonen, "Mid-infrared optical parametric oscillators and frequency combs for molecular spectroscopy," *Phys. Chem. Chem. Phys.* **18**(6), 4266–4294 (2016).
11. S. Bretschneider, C. Eggeling, and S. W. Hell, "Breaking the diffraction barrier in fluorescence microscopy by optical shelving," *Phys. Rev. Lett.* **98**(21), 218130 (2007).
12. K. T. Gahagan and G. A. Swartzlander, "Optical vortex trapping of particles," *Opt. Lett.* **21**(11), 827–829 (1996).
13. Z. Zhu et al., "Nonlinear optical trapping effect with reverse saturable absorption," *Adv. Photonics* **5**(4), 046006 (2023).
14. A. Forbes, "Structured light from lasers," *Laser. Photon. Rev.* **13**(11), 1900140 (2019).
15. J. C. Fang et al., "Optical orbital angular momentum multiplexing communication via inversely-designed multiphase plane light conversion," *Photonics Res.* **10**(9), 2015–2023 (2022).
16. D. Naidoo et al., "Intra-cavity generation of superpositions of Laguerre–Gaussian beams," *Appl. Phys. B* **106**, 683–690 (2012).
17. N. R. Heckenberg et al., "Generation of optical phase singularities by computer generated holograms," *Opt. Lett.* **17**(3), 221–223 (1992).
18. G. A. Turnbull et al., "The generation of free-space Laguerre-Gaussian modes at millimetre-wave frequencies by use of a spiral phase plate," *Opt. Commun.* **127**(4-6), 183–188 (1996).
19. R. J. Li et al., "Generating large topological charge Laguerre–Gaussian beam based on 4K phase-only spatial light modulator," *Chin. Opt. Lett.* **20**(12), 120501 (2022).
20. W. Koechner, *Solid-State Laser Engineering*, 6th ed., pp. 211–231, Semantic Scholar (2006).
21. A. Ito, Y. Kozawa, and S. Sato, "Generation of hollow scalar and vector beams using a spot-defect mirror," *J. Opt. Soc. Am. A* **27**(9), 2072–2077 (2010).
22. Y. F. Chen and Y. P. Lan, "Dynamics of the Laguerre Gaussian TEM0,ℓ* mode in a solid-state laser," *Phys. Rev. A* **63**(6), 063807 (2001).
23. Y. F. Chen and Y. P. Lan, "Dynamics of helical-wave emission in a fiber-coupled diode end-pumped solid-state laser," *Appl. Phys. B* **73**(1), 11–14 (2001).
24. Z. Qiao et al., "Generating high-charge optical vortices directly from laser up to 288th order," *Laser Photonics Rev.* **12**(8), 1800019 (2018).
25. Q. Sheng et al., "Intracavity spherical aberration for selective generation of single-transverse-mode Laguerre-Gaussian output with order up to 95," *PhotoniX* **3**(1), 4 (2022).
26. Q. Sheng et al., "Ultra-high-order Laguerre-Gaussian field generated directly from a laser cavity with spherical aberration," *Laser Photonics Rev* **17**(8), 2300369 (2023).
27. A. J. Lee, T. Omatsu, and H. M. Pask, "Direct generation of a first-Stokes vortex laser beam from a self-Raman laser," *Opt. Express* **21**(10), 12401–12409 (2013).
28. Y. J. Miao, L. Zhang, and J. Dong, "Broadband petal-like Raman laser," *Ann. Phys.* **534**(4), 2100476 (2022).
29. M. Martinelli et al., "Orbital angular momentum exchange in an optical parametric oscillator," *Phys. Rev. A* **70**(1), 013812 (2004).
30. T. Yusufu et al., "Tunable 2-μm optical vortex parametric oscillator," *Opt. Express* **20**(21), 23666–23675 (2012).
31. M. Ababaike et al., "Near and mid-infrared optical vortex parametric oscillator based on KTA," *Sci. Rep.* **11**(1), 1–6 (2021).
32. A. Aadhi et al., "Controlled switching of orbital angular momentum in an optical parametric oscillator," *Optica* **4**(3), 349–355 (2017).
33. A. Abulikemu et al., "Mid-infrared idler-resonant optical vortex parametric oscillator based on MgO:PPLN," *Opt. Laser Technol.* **171**, 110341 (2024).
34. D. Jashaner, Y. X. Zhou, and T. Yusufu, "Widely-tunable mid-infrared ($2.6-5$ μm) picosecond vortex laser," *Appl. Phys. Express* **15**, 102004 (2022).
35. Y. X. Zhou et al., "Generation of tunable, non-integer OAM states from an optical parametric oscillator," *Appl. Phys. Lett.* **122**(12), 121106 (2023).
36. P. Vaity, J. Banerji, and R. P. Singh, "Measuring the topological charge of an optical vortex by using a tilted convex lens," *Phys. Lett.* **377**(15), 1154–1156 (2013).
37. M. Okida et al., "Direct generation of high power Laguerre-Gaussian output from a diode-pumped Nd:YVO_4 1.3-μm bounce laser," *Opt. Express* **15**(12), 7616–7622 (2007).
38. J. W. Kim et al., "High power Er: YAG laser with radially-polarized Laguerre-Gaussian (LG01) mode output," *Opt. Express* **19**(15), 14526–14531 (2011).
39. R. L. Phillips and L. C. Andrews, "Spot size and divergence for Laguerre Gaussian beams of any order," *Appl. Opt.* **22**(5), 643–644 (1983).
40. J. W. Kim and W. A. Clarkson, "Selective generation of Laguerre–Gaussian (LG0n) mode output in a diode-laser pumped Nd: YAG laser," *Opt. Commun.* **296**, 109–112 (2013).
41. S. Y. Luo et al., "Power scaling of blue-diode-pumped Pr:YLF lasers at 523.0, 604.1, 606.9, 639.4, 697.8 and 720.9 nm," *Opt. Commun.* **380**, 357–360 (2016).

Yuxia Zhou is a PhD in the School of Chemistry and Chemical Engineering, Xinjiang Normal University, China, and also belongs to the Xinjiang Key Laboratory for Luminescence Minerals and Optical Functional Materials.

Xining Yang received her PhD in testing and measurement technology and instruments from Harbin University of Science and Technology, China, in 2020. She is currently a professor at the Xinjiang Key Laboratory for Luminescence Minerals and Optical Functional Materials, Xinjiang Normal University, China. Her research focuses on solid lasers.

Jianqiang Ye received his BS degree in applied physics from Jiangsu University of Science and Technology, China, in 2022. He is currently an MS student at the Xinjiang Key Laboratory for Luminescence Minerals and Optical Functional Materials, Xinjiang Normal University,

China. His research focuses on optical vortices, optical parametric oscillators, and amplifiers.

Yuanyuan Ma received her PhD in optical engineering from the Graduate School of Advanced Integration Science, Chiba University, Japan, in 2020. She is currently a postdoctoral research fellow in the Graduate School of Engineering at Chiba University. Her research area focuses on structured-light beam generation and solid-state Raman lasers.

Ying Wan received her PhD in communication and information systems from Shanghai University, China, in 2022. She is currently a lecturer at Nanjing University of Information and Technology, China. Her research interests focus on optical fiber and nonlinear frequency conversion.

Jianxiang Wen received his PhD in communication and information systems from Shanghai University, Shanghai, China, in 2011. Currently, he is an associate professor at Shanghai University. His current research interests include special optical fiber structure design, research, and preparation.

Taximaiti Yusufu received his PhD in optical engineering from the Graduate School of Advanced Integration Science, Chiba University, Japan, in 2014. He is currently a professor at the Xinjiang Key Laboratory for Luminescence Minerals and Optical Functional Materials, Xinjiang Normal University, China. His current research interests include optical vortices, OAM, structured light, nonlinear optics, optical parametric oscillators, and amplifiers.